

1 **Title: Force transmission is a master regulator of mechanical cell competition**

2
3 **Authors:** Andreas Schoenit^{1,#}, Siavash Monfared^{2,#}, Lucas Anger^{1,#}, Carine Rosse^{1,3}, Varun
4 Venkatesh², Lakshmi Balasubramaniam¹, Elisabetta Marangoni⁴, Philippe Chavrier³, René-
5 Marc Mège^{1,*}, Amin Doostmohammadi^{2,*} & Benoit Ladoux^{1,5,6,*}

6
7 **Affiliations:**

8 ¹ Université Paris Cité, CNRS, Institut Jacques Monod, F-75013 Paris, France

9 ² Niels Bohr Institute, University of Copenhagen, Copenhagen, Denmark

10 ³ Institut Curie, Paris Université Sciences et Lettres, Sorbonne Université, CNRS, UMR144,
11 75005 Paris, France

12 ⁴ Translational Research Department, Institut Curie, PSL Research University, Paris, 75005,
13 France

14 ⁵ Department of Physics, Friedrich-Alexander Universität Erlangen-Nürnberg, Erlangen,
15 Germany

16 ⁶ Max-Planck-Zentrum für Physik und Medizin, Erlangen, Germany

17
18 # Equal contribution

19 * Corresponding authors

20
21 **Abstract:**

22 Cell competition is a tissue surveillance mechanism for eliminating unwanted cells and as
23 such is indispensable in development, infection and tumorigenesis. Although different
24 biochemical mechanisms are proposed, due to the dearth of direct force measurements,
25 how mechanical forces determine the competition outcome remains unclear. Here, using
26 *ex vivo* tissues and different cell lines, we have discovered an unknown form of cell
27 competition that is regulated by differences in force transmission capabilities, favoring cell
28 types with stronger intercellular adhesion. Direct force measurements reveal increased
29 mechanical activity at the interface of the two competing cell types in the form of large
30 stress fluctuations which can lead to upward forces and cell elimination. We show how a
31 winning cell type endowed with a stronger intercellular adhesion exhibits a higher
32 resistance to elimination while benefiting from efficient force transmission to neighboring
33 cells. This cell elimination mechanism could have broad implications of keeping strong force
34 transmission ability for maintaining tissue boundaries and cell invasion pathology.

35
36 **Main text:**

37 Cell competition plays a vital role in maintaining tissue health, fighting against pathogens and
38 tumorigenesis ^{1–4}. Despite these widespread and crucial implications, the fundamental
39 principles that govern cell competition remain unclear. The elimination of loser cells can be
40 facilitated by biochemical signals, which lead to cell death and subsequent removal ^{1,2}, but
41 various studies have also shown that cells can mechanically outcompete each other ^{5,6}. The

42 prevailing consensus is that winners compress losers, promoting loser cell's death and
43 removal^{3,5,6}. Different strategies such as directed migration^{7,8}, crowding⁹, differences in cell
44 growth^{10,11} or homeostatic density^{12,13} enable winning cells to apply pressure or resist to it
45^{7–13}. However, contradicting outcomes have emerged from studies exploring the change of
46 cell mechanics through modulating the extracellular environment^{14–16} or changing
47 contractility, e.g. by overexpressing the oncogene Ras^{V12} in different *in vivo* and *in vitro*
48 systems^{17–23}. Although cell competition is involved in various biological and pathological
49 processes, a framework that integrates the role of collective mechanical interactions in cell
50 competition is lacking. In particular, if and how cell competition is influenced by the
51 fundamental process of intercellular force transmission is not known. Sensing, transmitting
52 and exerting mechanical forces between cells is mediated in epithelia by the adherens
53 junction protein E-cadherin²⁴, which is crucial for efficient intercellular mechanical coupling
54^{25–30}. Therefore, we conjectured that altering the intercellular force transmission through
55 modifying the E-cadherin adhesion strength could lead to the emergence of cell competition
56 and could strongly affect its outcome.

57

58 ***Cells with higher intercellular force transmission capabilities win in cell competition***

59 We set out to investigate if heterogeneities in intercellular adhesion strength and
60 consequently force transmission capabilities could lead to competitive interactions. A
61 pathological example of such molecular heterogeneities can be found in metaplastic breast
62 cancers, a highly aggressive triple-negative breast cancer subtype presenting a therapeutic
63 challenge³¹. The intra-tumoral heterogeneity in force transmission capability is recapitulated
64 by the presence of at least two sub-populations of cancer cells, epithelial and mesenchymal
65³¹, with potentially varying E-cadherin expression levels in epithelial sub-population³². To
66 address how tumor cell subclones sorted and if they competed within a tumor, we cultivated
67 patient-derived xenografts from metaplastic breast cancers and monitored their
68 development. To focus on the role of force transmission capabilities in cell competition, we
69 chose xenografts with a binary state in E-cadherin expression, i.e. in which E-cadherin is
70 strongly expressed in the epithelial, but absent in the mesenchymal sub-population. The two
71 sub-populations sorted, resulting in clusters of E-cadherin-positive epithelial cells (E-cad⁺)
72 surrounded by E-cadherin-negative mesenchymal cells (E-cad⁻) (**Fig. 1a**). We further observed
73 a competition between the cell types: over time, the E-cad⁺ clusters expanded at the cost of
74 E-cad⁻ cells, removing them from the substrate (**Fig. 1b**, Video 1). This increased removal of
75 E-cad⁻ cells was only observed when both sub-populations directly interacted (**Fig. S1 A**). We
76 confirmed our observations using cells from a second breast cancer patient (**Fig. S1 B,C**, Video
77 2). These observations indeed suggests that heterogeneities in intercellular adhesion strength
78 can lead to cancer cell competition, in which cells with increased adhesion strength win.
79 To investigate the role of intercellular adhesion in cell competition more systematically, we
80 turned to competition between two other cell types: we lowered the adhesion strength of
81 MDCK epithelial cells by knocking out E-cadherin (E-cad KO). In pure cultures, E-cad KO cells
82 showed no signs of reduced cell viability and due to the presence of cadherin 6, they still form

83 mechanically active junctions, although of lower strength³³. Mixing E-cad KO and WT cells,
84 we observed that the populations sorted^{33,34} and that the E-cad KO cells were outcompeted
85 by the WT cells (**Fig. 1c**). Because both cell types showed a similar cell density (**Fig. S2 A**), we
86 used population area change to estimate cell losses. To quantify population areas, E-cad KO
87 cells were expressing lifeAct-GFP. These cells lost against normal WT cells as well as WT cells
88 expressing lifeAct-mCherry (**Fig. S2, B**), excluding an impact of lifeAct expression on the
89 competition. Importantly, E-cad KO cell loss was independent of cell ratios, as they also lost
90 when in majority (**Fig. S2 C**). To better control the boundary between the two cell types, we
91 developed a collision assay of two migrating cell populations^{18,35} which led to the same
92 competition outcome (**Fig. S2 C**, Video 3). To assess if and how E-cad KO cells compete against
93 cells with even further reduced cell-cell adhesion, we mixed them with MDCK E-
94 cadherin/cadherin 6 double knockout cells (dKO) which cannot form any adherens junctions
95³⁶. The previously losing E-cad KO cells won and outcompeted the dKO cells (**Fig. 1d**, Video 4).
96 To modulate force transmission strength through the expression levels of E-cadherin, we then
97 mixed WT and E-cadherin overexpressing³⁷ (E-cad OE) cells. WT cells were eliminated by
98 these cells with even further increased cell-cell adhesion (**Fig. S3 A-D**). To generalize our
99 findings, we performed similar experiments with another epithelial cell line which originates
100 from breast tissue, MCF10A cells, mixing WT and E-cad KO cells³⁸. The E-cad KO cells were
101 also eliminated by the WT cells, both in mixed cultures (**Fig. S3 E**) and in collision assays (**Fig.**
102 **S3 F**). Taken together, experiments across diverse cell types show, without exception, that
103 cells with relatively stronger adherens junctions always win in cell competition, including
104 patient-derived tumors and various epithelial cell lines.
105

106 ***Winning cells can be under tensile or compressive stresses***

107 Cell elimination can be governed in epithelia by compressive stresses³⁹⁻⁴¹. As force
108 transmission within tissues is mainly regulated through adherens junctions^{25,27,42}, we first
109 reasoned that stronger intercellular adhesion could allow winning cells to collectively exert
110 compressive stresses on the losing cells, in line with current consensus described in the
111 literature^{7-9,11-13,17}. Unlike previous studies, our experimental setup provides additional
112 information that includes direct access to intercellular stresses using Bayesian Inversion Stress
113 Microscopy^{41,43,44}. In the patient-derived tumor cultures, we observed that the winning E-
114 cad⁺ cells were under high levels of tension and the losing E-cad⁻ cells under compression (**Fig.**
115 **1e**), in agreement with their strong differences in stiffness (**Fig. S4 A,B**) and exerted traction
116 forces (**Fig. S4 C**). However, to our surprise in mixtures of MDCK WT and E-cad KO cells,
117 winning WT cells were under compression and losing E-cad KO cells were under tension (**Fig.**
118 **1f**). This non-intuitive, unanticipated, observation is contrary to established models^{7-9,11-13,17}.
119 We confirmed this result with the collision assay in which we controlled temporally the
120 establishment of the contact between the two cell types. The mechanical state of WT cells
121 switched from tensile during migration to compressive after the collision with the E-cad KO
122 cells (**Fig. S5 A**). Similar results were obtained using another force interference method
123 independent of traction forces and based on cell shape obtained from labelling tight junctions

124 ⁴⁵ (**Fig. S5 B,C**). They were further confirmed by laser ablation experiments (**Fig. S5 D**), were
125 WT cells showed a negative (Video 5, compression) and E-cad KO cells a positive recoil (Video
126 6, tension) (**Fig. S5 E**). Although E-cad KO cells were on average under tension, local regions
127 remained under compression (**Fig. 1f**). Thus, we wondered whether E-cad KO cells were
128 eliminated preferentially at these local compressive regions. Assessing the isotropic stresses
129 locally (**Fig. S6 A,B**) prior to cell elimination revealed that E-cad KO cells were under tension
130 before and during the elimination process (**Fig. S6 C**). This confirms that the competition
131 outcome is independent of local compressive regions. To further compare this mechanism to
132 previously established cell competition scenarios that include loser cell death^{7,9,10}, we
133 investigate the fate of eliminated cells by labelling dying cells with annexin V. We observed
134 that 70% of E-cad KO cells were eliminated alive and only later died due to their extraction
135 from the tissue and thus the absence of adhesion⁴⁶ (**Fig. S6 D,E**). Furthermore, we inhibited
136 apoptosis using a pan-caspase inhibitor, which did not change the competition outcome (**Fig.**
137 **S6 F**). Together, this data shows that the cell elimination mechanism is independent of loser
138 cell death. Moreover, since cell competition based on biochemical signaling usually leads to
139 cell death^{1,2}, live cell extrusion strongly supports a cell elimination mechanism based on
140 mechanical forces.

141 To investigate other competition scenarios, we changed the mechanical environment of all
142 cells using softer substrates (370 Pa) to lower the cell-substrate adhesion⁴⁴ (**Fig. S7 A**) and
143 exerted tractions (**Fig. S7 B**). Under such conditions, E-cad KO cells were now under
144 compression and the WT cells under tension (**Fig. 1g**) but the competition outcome remained
145 the same, i.e. WT cells won independently of substrate composition or stiffness (**Fig. 1h**). We
146 further measured stresses in the competition between E-cad KO and dKO cells and observed
147 the same pattern of tension-compression with winners, E-cad KO cells, under tension and
148 losers, dKO cells, under compression (**Fig. 1i**). Overall, we show that compression-induced cell
149 loss can indeed explain the outcome of different competition scenarios. However, the direct
150 measurement of intercellular stresses challenges this established consensus that winners
151 always squeeze out losers. Demonstrating that cells can be under compression and still win
152 suggests that other, still unknown mechanisms must be governing the cell competition
153 outcome.

154

155 ***Elimination of E-cad KO cells cannot be explained by any established mechanism***

156 To understand why the E-cad KO cells were losing despite being under tension, we first ruled
157 out previously conjectured mechanisms. For instance, differential cell growth could impact
158 cell competition^{11,12,10}, but both cell types exhibited identical fractions of mitotic cells (**Fig.**
159 **S8 A**) and similar growth rates (**Fig. S8 B**) in pure and mixed cultures. Cells with higher
160 homeostatic density can have a competitive advantage^{13,7}, but cell competition emerged at
161 cell densities well below the homeostatic density of both cell types (**Fig. S8 C**). Quantifying
162 the rates of cell elimination, both cell types showed similar extrusion rates in pure cultures,
163 and the rates increased with time and cell density (**Fig. S8 D**). In mixed cultures, however, the
164 rate of extrusion was strongly increased for E-cad KO cells compared to pure cultures, and

165 independent of cell density, while the rate of extrusion for WT cells remained comparable to
166 pure cultures (**Fig. 2a**, **Fig. S8 D**). This demonstrates that the predominant elimination of E-
167 cad KO cells in mixed cultures was not due to cell-intrinsic processes but resulted from their
168 collective interactions with WT cells. Previous reports on the role of cell mechanics in cell
169 competition have conjectured that a relative increase in cell-substrate adhesion^{8,16} and cell
170 stiffness^{12,17} provides a competitive advantage. Furthermore, E-cadherin based adherens
171 junctions have shown to be mechanosensitive, affecting various aspects of cell and tissue
172 mechanics^{26,33,47-49}. Thus, we assessed how the decrease of cell-cell adhesion strength (**Fig.**
173 **S9 A,B**) had globally affected E-cad KO cell mechanics. The cells capacity to form tight- or
174 desmosome junctions was not changed (**Fig. S5 B**; **Fig. S9 C**). This underlines that the
175 mechanical link between the cells is only weakened. In mixed cultures, E-cad KO cells exerted
176 significant larger traction forces on the substratum than their WT counterparts (**Fig. S9 C**) and
177 showed a striking increase in focal adhesion size (**Fig. 2b**, **Fig. S9 D**). Using surface indentation,
178 we measured a significant increase in E-cad KO cell stiffness compared to WT cells for pure
179 and mixed cultures (**Fig. S9 E**), most likely due to their more prominent actin-based contractile
180 phenotype³³ (**Fig. 2c**). These observations demonstrate that a cell population's ability to
181 generate increased forces and exert them on competing cells does not necessarily provide a
182 competitive advantage: Loser cells can exhibit stronger cell-substrate adhesions and higher
183 stiffness, which explains the state of tension in eliminated E-cad KO cells, but make their
184 elimination even more puzzling, contradicting the proposed cell-substrate and cell stiffness
185 advantage^{8,12,16,17}. Finally, contact-dependent cell-cell signaling could lead to cell elimination
186 independent of mechanical forces^{1,2}. However, we observed that E-cad KO cells were
187 eliminated not only at the interface of the two populations, but also more than one cell row
188 away from it (**Fig. S10 A**, Video 7). In conclusion, having tested multiple possibilities, we ruled
189 out the applicability of previously reported mechanisms in explaining the outcome of WT and
190 E-cad KO cell competition, suggesting that a new, hitherto unknown, mechanism must be at
191 play.
192

193 ***Cell elimination is localized at a mechanically active interface***

194 To further explore the preferred elimination of E-cad KO cells, we investigated the spatial
195 distribution of extrusion events. Previous studies on mechanical cell competition proposed
196 that loser cells get eliminated in the bulk of the cell cluster, where compressive stress is the
197 highest⁶. Moreover, increased contractility at tissue interfaces can impact cell elimination
198 during development^{20,22}, but its role remains elusive²¹. We found that the losing E-cad KO
199 cells were preferentially eliminated near the interface, while the WT cell extrusions showed
200 a relatively homogenous distribution (**Fig. 2d**). The WT cells did not show an increased cell
201 density at the interface (**Fig. S10B**); thus, E-cad KO extrusions were independent of local WT
202 densities. Importantly, neither the free edge of isolated E-cad KO monolayers (**Fig. S10 C**) nor
203 an interface of a confined E-cad KO layer with a rigid passive fence (**Fig. S10 D**) recapitulated
204 the predominant localization of extrusions at the interface. This suggests that the preferred
205 elimination of E-cad KO cells is triggered by the active interface that emerges between the

206 two tissues with contrasting mechanical properties. Accordingly, the shared interface of E-
207 cad KO and WT cells was strongly enriched in phosphorylated actomyosin in both cell types
208 (**Fig. 2e,f, Fig. S11 A**), indicating an increased mechanical activity there. LifeAct and phospho-
209 myosin colocalized (**Fig. S11 A**). Using live cell imaging, we observed a polarization in actin
210 accumulation only at the shared interface the cell types first collided (**Fig. S11 B**), which
211 underlines the increased interface force generation. In this vein, we extended our analysis to
212 the patient-derived tumor cultures. As in MDCK cells, the losing E-cad⁻ cells were extruded at
213 the tissue interface (**Fig. S11 C**), where increased actomyosin activity was observed (**Fig. S11**
214 **D**). MDCK WT cells could even form pluricellular actomyosin cables at areas of high negative
215 curvature (**Fig. 2f**). We hypothesized that pluricellular formation of actomyosin cables might
216 help WT cells in efficiently removing small E-cad KO clusters through purse-string mechanisms
217 as observed in wound closure ²⁴. However, E-cad KO cells got eliminated at both regions of
218 positive and negative curvatures (**Fig. S12**). Thus, such cables cannot be a dominant factor
219 here. Independently of curvature, the enrichment in active myosin could generate a
220 mechanical barrier, which prevents mixing of cell types through which they might confine
221 each other ²⁰. Together, the correlation between cell elimination and high mechanical activity
222 suggests a critical role of this active interface in determining the outcome of cell competition.
223 We then postulated that cell types endowed with different mechanical properties might react
224 differently to this increased interface activity. To predict how energetically costly it is to
225 eliminate each cell type, we considered a simplified analytical model for energetic
226 requirements of cell elimination: at the interface, two competing cells pull and push on each
227 other leading to deformations of the cells. Thus, the work done on each cell type to deform
228 and eventually eliminate it can be expressed in terms of the energies associated with cell-
229 substrate and cell-cell adhesions strengths, and cell stiffness (see Methods). The energy
230 required to remove a cell can be simply estimated as the work required to deform the cell
231 from a cylindrical shape to a cone-like shape and then rounding it up to a sphere upon cell
232 removal (**Fig. S13**). Comparing the work required to eliminate the competing cells as a
233 function of the difference in their cell-cell adhesion strength demonstrates that the cell type
234 with a higher cell-cell adhesion could require more work to be eliminated, even if the other
235 type has a higher cell-substrate adhesion (**Fig. 2g**). This simple energetic argument shows that
236 the energy barrier for elimination is higher for cells with strong cell-cell adhesion. As such,
237 this minimal model, does not consider where the energy required for elimination comes from
238 and therefore does not tell anything about the mechanism driving the elimination. To bridge
239 this gap, we next employ a more detailed, cell-based model that resolves individual cells, their
240 interactions, and mechanics.

241

242 **A computational model reveals stress fluctuations lead to interfacial cell elimination**

243 To understand how the active interface affects mechanical competition and why strong cell-
244 cell adhesion presents a competition advantage therein, we turned to physical modeling of
245 3D cell monolayers ⁵⁰. Our model is based on a multi-phase fields approach that accounts for
246 both passive and active interactions of deformable cells in three-dimensions (3D). These

247 interactions include cell-cell and cell-substrate adhesion strengths that are considered
248 explicitly and tuned independently (see **Fig. S14** for model schematics). This enables
249 modulating force transmission capability and its effect on the competition outcome while
250 providing access to the out-of-plane 3D stress components that govern the removal of cells
251 from a monolayer (see Methods). A cell extrusion is captured in the model without any explicit
252 threshold, or external artificial means to favor one. Once the out-of-plane forces acting on a
253 cell overpower the forces keeping it in the monolayer and on the substrate, a cell extrusion
254 occurs. In this vein, the collective behavior of cells, e.g. cell extrusion and height fluctuations,
255 emerge from solving the dynamics associated with translation and interface relaxation of
256 each cell (see Methods) (**Fig. S15**). To best represent the experimental conditions, we
257 modeled collision assays of two model cell types (**Fig. 3a**, Video 8): model wild type (mWT),
258 and model E-cad KO (mE-cad KO) defined based on cell-cell adhesion differences (lower for
259 mE-cad KO) and/or cell-substrate adhesion contrast (higher for mE-cad KO). In agreement
260 with the experimental observations, mE-cad KO cells, with a higher cell-substrate adhesion
261 and a lower cell-cell adhesion relative to mWT cells, were eliminated at the interface (**Fig. 3b**).
262 To understand why E-cad KO cells are eliminated at the interface, we quantified the
263 fluctuations in stress fields *via* susceptibility^{51,52}, which is defined as $\chi = N \times [\langle \sigma^2 \rangle -$
264 $\langle \sigma \rangle^2]$, where $\langle \rangle$ indicates expectation and N is the number of data points corresponding to
265 σ, σ^2 fields. The susceptibility of isotropic stress field primarily due to in-plane fluctuations
266 (**Fig. S16**), $\chi_{\sigma_{2D}^{iso}}$, and linked to out-of-plane component of stress tensor, σ_{zz} , peaked at the
267 interface of mE-cad KO and mWT cells, a consequence of contrasting physical properties of
268 the cell types considered (**Fig. 3c**). At the same time, in-plane stress fields exhibited a weaker
269 correlation in mE-cad KO cells relative to mWT cells, suggesting a muted ability to transmit
270 stresses (**Fig. 3d**). Additionally, the out-of-plane component of the stress field, σ_{zz} , near the
271 interface exhibited a pronounced localization in mE-cad KO cells relative to their mWT
272 counterparts (**Fig. 3e**), particularly in the tensile region (**Fig. 3f**). To further investigate the link
273 between in-plane fluctuations and out-of-plane stress localization, we considered a series of
274 simulations where cell-substrate adhesion contrast is kept constant, while the contrast in cell-
275 cell adhesion is increased, by reducing the cell-cell adhesion strength of mE-cad KO cells.
276 Interestingly, in-plane susceptibility near the interface decreased (**Fig. 3g**) while the location
277 of extrusion events shifted away from the interface (**Fig. 3h**) as the contrast in cell-cell
278 adhesion is reduced. These results suggested that higher in-plane fluctuations led to more
279 extrusions of mE-cad KO cells near the interface. To understand why, we focused on stress
280 transmission away from the interface.

281 We noted a more persistent susceptibility away from the interface i.e. a relatively smaller
282 difference in susceptibility near the interface and further from it, by increasing cell-cell
283 adhesion (**Fig. 3g**). More importantly, characterization of the spatial correlation of averaged,
284 in-plane, isotropic stress fields prior to and at the onset of extrusion (**Fig. 3i**) showed that
285 these fields became more correlated as the cell-cell adhesion of mE-cad KO cells are
286 increased, signaling a more efficient transmission of mechanical information. Indeed,
287 inspection of the out-of-plane component of the averaged fields, σ_{zz} , around extrusions show

288 higher localization due to ineffective stress transmission by mE-cad KO cells with low cell-cell
289 adhesion (**Fig. 3j**), resulting mE-cad KO cells to extrude near the interface. In summary, the *in*
290 *silico* study showed (i) the emergence of an actively fluctuating interface due to differences
291 in cell-cell adhesion strengths and (ii) weakening cell-cell adhesion hindered the flow of
292 mechanical information away from this active interface, manifesting in less correlated stress
293 fields. This explained why mE-cad KO cells are eliminated at the interface. Unable to transmit
294 the high in-plane isotropic stress fluctuations away from the interface, mE-cad KO cells seek
295 relief by localizing stresses out-of-plane and potentially extruding as mWT cells expand into
296 their domain.
297

298 ***Experiments confirm strong interface stress fluctuations driving cell elimination***

299 To verify these predictions, we first assessed experimentally the susceptibility of mechanical
300 stresses and found the same striking increase of stress fluctuations at the interface, which
301 correlates with the localization of E-cad KO extrusions (**Fig. 4a**). As expected, the increase of
302 fluctuations at the interface was also found in the substrate displacement and in the traction
303 forces (**Fig. S17 A**). Additionally, in line with simulation predictions of enhanced fluctuations
304 at higher cell-cell adhesion difference, we observed even stronger interface fluctuations in
305 the primary tumor sample where the difference in cell-cell adhesion is higher relative to
306 MDCK cells (**Fig. S17 B**). Besides differences in cell-cell adhesion, we hypothesized that high
307 cellular activity is required for high stress and traction fluctuations. To investigate cellular
308 behavior at the interface, we assessed the dynamics of the actin cytoskeleton. E-cad KO cells
309 were highly active and extended several μm long protrusions below surrounding WT cells (**Fig.**
310 **4b**, Video 9). This dynamic protrusion activity demonstrated an increased cellular motility of
311 E-cad KO cells at the interface, in line with increased traction fluctuations. We inhibited
312 protrusion formation using CK666. E-cad KO cells did not lose any more (**Fig. S17 C**), which
313 additionally supports that interface fluctuations are crucial for their elimination. Furthermore,
314 increased mechanical activity could lead to increased stress fluctuations. To reduce the
315 mechanical activity, we treated MDCK cells with blebbistatin. It globally inhibits actomyosin-
316 generated cellular forces, which might have variable effects on the entire cell population.
317 Blebbistatin disrupted the interface between the cells, evident by a reduced interface
318 convexity (**Fig. 4c**, **Fig. S18 A, B**). Importantly, blebbistatin decreased stress magnitudes (**Fig.**
319 **S18 C**), leading to cell relaxation ⁵³. Due to their increased contractility, this relaxation is
320 relatively stronger in E-cad KO cells, increasing the area of single cells (**Fig. S18 D**), and leading
321 to an E-cad KO domain increase after blebbistatin addition (**Fig. S18 E**). The reduction of
322 cellular forces led to a striking drop in stress fluctuations (**Fig. 4d**), which correlated with a
323 significant reduction in the global extrusion rate of E-cad KO cells, while the extrusion rate for
324 WT cells remained the same (**Fig. S18 F**). These experiments confirm the emergence of
325 increased stress fluctuations at mechanically active tissue interfaces and indicate that
326 maintaining the active interface is required for WT cells winning.
327 To further explore the relationship between interface stress fluctuations and cell elimination,
328 we assessed the local stress fields before cell extrusions close to the interface by computing

329 the ensemble average stresses up to 40 min before the extrusion event. The stress field
330 around cell extrusion events in E-cad KO cells exhibited high values of both compressive and
331 tensile stresses (**Fig. 4e, left**) whereas the one at random positions at the interface were under
332 lower values of tensile stresses (**Fig. 4e, right**). This indicates that E-cad KO cells experienced
333 increased fluctuations of stresses prior to their elimination at the interface. By contrast, the
334 stress field around extruding WT cells, which showed no preference for being eliminated at
335 the interface (see **Fig. 2**), was exclusively compressive (**Fig. 4f**). These findings are confirmed
336 by the distribution of isotropic stresses, which showed a much wider range and more extreme
337 values of both compressive and tensile stresses for E-cad KO cells destined to extrude
338 compared to E-cad KO cells at random positions (**Fig. 4g**). We next analyzed the temporal
339 evolution of local stress fluctuations up to 60 min prior to extrusion and compared them to
340 fluctuations at random positions along the interface. While the fluctuations at random
341 positions and for WT cells remained relatively stable, we observed a strong and significant
342 increase starting 40 min before E-cad KO cell extrusion events (**Fig. 4h, Fig. S19 A**). Post
343 removal, these fluctuations returned to the initial level (**Fig. 4h**). Together, these different
344 mechanical signatures of cell elimination point towards different cell elimination
345 mechanisms: WT cells are extruded through high compressive stresses ^{39–41}. In contrast to
346 that, we found another cell elimination mechanism as E-cad KO cells are eliminated at the
347 interface through increased stress fluctuations. In the competition between two cell types,
348 this latter mechanism based on stress fluctuations can be dominant and governs the
349 outcome.

350

351 ***Collective stress transmission and deformation prevent cell elimination***

352 Cells at the interface were subjected to increased stress fluctuations, but only the ones with
353 lower intercellular adhesion were eliminated. Therefore, we reasoned that high intercellular
354 adhesion must endow the winning ones with mechanisms to resist stress fluctuation-
355 mediated elimination. The computational model predicted more efficient stress transmission
356 to neighboring cells, preventing the localization of out-of-plane stresses in winning cells (**Fig.**
357 **3d-f**). Indeed, WT cells showed a significantly increased stress correlation length compared to
358 E-cad KO cells (**Fig. 5a, b**). This confirms a more efficient transmission of mechanical stress to
359 neighboring cells for WT cells. The observation of multicellular actomyosin cables between
360 WT cell (see **Fig 2**) but not between E-cad KO cells (**Fig. S19 B**) supports these measurements.
361 Furthermore, we reasoned that the proposed mechanism of stress fluctuations at the
362 interface should be reflected in deformations and changes in cell shape. To this end, we
363 assessed the cell height and the cell-cell adhesion area of WT and E-cad KO cells. Although
364 both cell types normally have the same height (**Fig. 5c, top**), cell shapes fluctuated near the
365 interface and particularly, WT cells could morph into columnar shape (**Fig. 5c, bottom**). The
366 differences in cell shapes on the collective level were most striking in the collision assay,
367 where the WT cell deformation started from the boundary and extended over multiple cells
368 into the bulk. However, the E-cad KO cells did not deform collectively and cells away from the
369 interface remained flat (**Fig. 5d, e**). The WT cells strongly deformed within the first 12 hours

370 following collision (**Fig S19 B,C**), which correlated well with the increasing E-cad KO extrusion
371 rate (**Fig S19 D**). Moreover, when surrounded by E-cad KO cells, islands of WT cells could
372 collectively sustain high deformation and drastic cell area fluctuations over hours without
373 being extruded (**Fig. 5f**). Such cell shape changes thus increased the intercellular contact zone
374 between WT cells, allowing them to further increase their adhesive energy to better resist
375 stress fluctuations. Notably, some doublets of WT cells were eliminated by E-cad KO cells,
376 suggesting that isolated WT cells cannot propagate stresses and lose their advantage (**Fig S19**
377 **E**). The mirror situation revealed that islands of E-cad KO cells did not undergo such strong
378 deformations and released stresses through cell elimination by extrusion (**Fig. 5g**). Together,
379 these experiments confirmed enhanced stress transmission in winning cell types and further
380 show that keeping strong intercellular adhesion allows the winning type to resist elimination
381 through substantial cell shape deformations.

382

383 **Discussion**

384 Here, we discover that differences in force transmission capability directly determine the
385 outcome of mechanical cell competition, in which cells with stronger intercellular adhesion
386 are exclusively winning. Because no previously described cell elimination mechanism could
387 explain our observations, we propose a new one based on combining simulation and
388 experiments. We note that a possible contribution of secreted, extracellular factors to cell
389 elimination ¹ cannot be excluded completely. Comparing stress patterns across multiple
390 competition scenarios demonstrates that cells with increased force generation are under
391 tension, which compresses the other cell population. Because these stress patterns can not
392 predict winning and losing, we propose that the force transmission, rather than the force
393 generation capability governs the competition outcome. Thus, our proposed mechanism is
394 independent of loser cell compression ^{7–9,17,20} and differences in growth rate or homeostatic
395 density ^{11–13}. Increased fluctuations of isotropic stresses emerge at active interfaces between
396 tissues with different mechanical properties. These high fluctuations in local stress fields near
397 the interface, if not transmitted efficiently by the front-line cells to the rest of the collective,
398 localize and induce out-of-plane stresses, akin to Poisson effect in elasticity, which can lead
399 to cell elimination. In scenarios where cells with heterogeneities in force transmission
400 capability compete against each other, intercellular adhesion provides a generic winning
401 strategy since it enables winning cells to withstand higher fluctuations of stresses than losing
402 cells. Thus, unlike other forms of mechanical cell competition such as directed migration
403 towards losing cells ^{7,8,15}, our findings unveil an alternative mechanism based on active
404 resistance to elimination through a reinforcement of intercellular adhesion. Indeed, cells with
405 higher intercellular adhesion can transmit stresses more efficiently to neighboring cells which
406 prevents the localization of elimination-promoting out-of-plane stresses. In addition,
407 increased intercellular adhesion allows collective cell shape changes into a columnar shape,
408 which increases the mechanical threshold required for elimination through further increasing
409 the adhesive energy. By contrast, cells with relatively lower intercellular adhesion are
410 eliminated through the localization of high stress fluctuations at the interface and an overall

411 limited resistance to out-of-plane stresses (**Fig. 5h**). Our conclusions are based on a physical
412 model, only relying on the effect of mechanical imprints. Thus, if similar mechanical imprints
413 are given, this proposed framework could have important implications for different biological
414 processes beyond cell competition. Since it does not rely on loser cell death, it could play a
415 role in organizing tissues during morphogenesis. Force transmission differences could be
416 involved in maintaining tissue boundaries and, thus, functionality in homeostasis. In the skin,
417 for example, loser cells are expelled apically through an unknown mechanism, and failed
418 competition leads to deteriorated barrier function⁵⁵. The reduction of intercellular adhesion
419 has been associated with metastasis for a long time⁵⁶. Adding to these mechanisms,
420 increased stress fluctuations at the interface of tumoral and normal tissues could also play a
421 role in invasion mechanism or promote metastasis, if tumoral cells are eliminated alive^{6,57}.
422 Moreover, as suggested by our experiments using patient-derived tumor xenografts, this
423 mechanism of cell competition could be acting within tumors with heterogeneities in their
424 cell-cell adhesion strength. While this study is focused mainly on binary expression of
425 adhesion molecules, further studies need to address heterogeneity of Cadherin expression
426 levels, which are present in other breast cancers³². Mechanical cell competition might change
427 the fate of cells, *i.e.* promote invasion and subsequent metastasis of sub-populations. Thus,
428 it will be exciting to further explore the role of this form of cell competition in tissue sculpting
429 and different pathologies.
430

431 **References:**

- 432
- 433 1. Baker, N. E. Emerging mechanisms of cell competition. *Nature Reviews Genetics* **21**,
434 683–697 (2020).
- 435 2. van Neerven, S. M. & Vermeulen, L. Cell competition in development, homeostasis and
436 cancer. *Nature Reviews Molecular Cell Biology* (2022) doi:10.1038/s41580-022-00538-y.
- 437 3. Parker, T. M. *et al.* Cell competition in intratumoral and tumor microenvironment
438 interactions. *The EMBO Journal* **40**, e107271 (2021).
- 439 4. Vishwakarma, M. & Piddini, E. Outcompeting cancer. *Nature Reviews Cancer* **20**, 187–
440 198 (2020).
- 441 5. Brás-Pereira, C. & Moreno, E. Mechanical cell competition. *Current Opinion in Cell
442 Biology* **51**, 15–21 (2018).
- 443 6. Levayer, R. Solid stress, competition for space and cancer: The opposing roles of
444 mechanical cell competition in tumour initiation and growth. *Seminars in Cancer Biology*
445 **63**, 69–80 (2020).
- 446 7. Wagstaff, L. *et al.* Mechanical cell competition kills cells via induction of lethal p53
447 levels. *Nature Communications* **7**, 11373 (2016).
- 448 8. Bastounis, E. E. *et al.* Mechanical competition triggered by innate immune signaling
449 drives the collective extrusion of bacterially infected epithelial cells. *Developmental Cell*
450 **56**, 443-460.e11 (2021).
- 451 9. Levayer, R., Dupont, C. & Moreno, E. Tissue Crowding Induces Caspase-Dependent
452 Competition for Space. *Current Biology* **26**, 670–677 (2016).
- 453 10. Price, C. J. *et al.* Genetically variant human pluripotent stem cells selectively eliminate
454 wild-type counterparts through YAP-mediated cell competition. *Developmental Cell* **56**,
455 2455-2470.e10 (2021).

- 456 11. Shraiman, B. I. Mechanical feedback as a possible regulator of tissue growth.
- 457 *Proceedings of the National Academy of Sciences* **102**, 3318–3323 (2005).
- 458 12. Gradeci, D. *et al.* Cell-scale biophysical determinants of cell competition in epithelia.
- 459 *eLife* **10**, e61011 (2021).
- 460 13. Basan, M., Risler, T., Joanny, J., Sastre-Garau, X. & Prost, J. Homeostatic competition
- 461 drives tumor growth and metastasis nucleation. *HFSP Journal* **3**, 265–272 (2009).
- 462 14. Pothapragada, S. P., Gupta, P., Mukherjee, S. & Das, T. Matrix mechanics regulates
- 463 epithelial defence against cancer by tuning dynamic localization of filamin. *Nature Communications* **13**, 218 (2022).
- 464 15. Aparicio-Yuste, R., Muenkel, M., Clark, A. G., Gómez-Benito, M. J. & Bastounis, E. E.
- 465 A Stiff Extracellular Matrix Favors the Mechanical Cell Competition that Leads to
- 466 Extrusion of Bacterially-Infected Epithelial Cells. *Frontiers in Cell and Developmental Biology* **10**, (2022).
- 467 16. Nishio, M. *et al.* Hippo pathway controls cell adhesion and context-dependent cell
- 468 competition to influence skin engraftment efficiency. *The FASEB Journal* **33**, 5548–5560
- 469 (2019).
- 470 17. Moreno, E., Valon, L., Levillayer, F. & Levayer, R. Competition for Space Induces Cell
- 471 Elimination through Compaction-Driven ERK Downregulation. *Current Biology* **29**, 23-
- 472 34.e8 (2019).
- 473 18. Moitrier, S. *et al.* Collective stresses drive competition between monolayers of normal
- 474 and Ras-transformed cells. *Soft Matter* **15**, 537–545 (2019).
- 475 19. Hogan, C. *et al.* Characterization of the interface between normal and transformed
- 476 epithelial cells. *Nature Cell Biology* **11**, 460–467 (2009).
- 477 20. Porazinski, S. *et al.* EphA2 Drives the Segregation of Ras-Transformed Epithelial Cells
- 478 from Normal Neighbors. *Current Biology* **26**, 3220–3229 (2016).

- 481 21. Klipa, O., El Gammal, M. & Hamaratoglu, F. Elimination of aberrantly specified cell
482 clones is independent of interfacial Myosin II accumulation. *Journal of Cell Science* **136**,
483 jcs259935 (2023).
- 484 22. Bielmeier, C. *et al.* Interface Contractility between Differently Fated Cells Drives Cell
485 Elimination and Cyst Formation. *Current Biology* **26**, 563–574 (2016).
- 486 23. Kuromiya, K. *et al.* Calcium sparks enhance the tissue fluidity within epithelial layers
487 and promote apical extrusion of transformed cells. *Cell Reports* **40**, 111078 (2022).
- 488 24. Ladoux, B. & Mège, R.-M. Mechanobiology of collective cell behaviours. *Nature
489 Reviews Molecular Cell Biology* **18**, 743–757 (2017).
- 490 25. Kale, G. R. *et al.* Distinct contributions of tensile and shear stress on E-cadherin levels
491 during morphogenesis. *Nature Communications* **9**, 5021 (2018).
- 492 26. Noordstra, I. *et al.* An E-cadherin-actin clutch translates the mechanical force of cortical
493 flow for cell-cell contact to inhibit epithelial cell locomotion. *Developmental Cell* (2023)
494 doi:10.1016/j.devcel.2023.06.011.
- 495 27. Bazellières, E. *et al.* Control of cell–cell forces and collective cell dynamics by the
496 intercellular adhesome. *Nature Cell Biology* **17**, 409–420 (2015).
- 497 28. Perez-Vale, K. Z. *et al.* Multivalent interactions make adherens junction–cytoskeletal
498 linkage robust during morphogenesis. *Journal of Cell Biology* **220**, e202104087 (2021).
- 499 29. Malinverno, C. *et al.* Endocytic reawakening of motility in jammed epithelia. *Nature
500 Materials* **16**, 587–596 (2017).
- 501 30. Ollech, D. *et al.* An optochemical tool for light-induced dissociation of adherens
502 junctions to control mechanical coupling between cells. *Nature Communications* **11**, 472
503 (2020).
- 504 31. Reddy, T. P. *et al.* A comprehensive overview of metaplastic breast cancer: clinical
505 features and molecular aberrations. *Breast Cancer Research* **22**, 121 (2020).

- 506 32. Zhang, Y., Toy, K. A. & Kleer, C. G. Metaplastic breast carcinomas are enriched in
507 markers of tumor-initiating cells and epithelial to mesenchymal transition. *Modern*
508 *Pathology* **25**, 178–184 (2012).
- 509 33. Balasubramaniam, L. *et al.* Investigating the nature of active forces in tissues reveals how
510 contractile cells can form extensile monolayers. *Nature Materials* **20**, 1156–1166 (2021).
- 511 34. Steinberg, M. S. & Takeichi, M. Experimental specification of cell sorting, tissue
512 spreading, and specific spatial patterning by quantitative differences in cadherin
513 expression. *Proceedings of the National Academy of Sciences* **91**, 206–209 (1994).
- 514 35. Vedula, S. R. K. *et al.* Emerging modes of collective cell migration induced by
515 geometrical constraints. *Proceedings of the National Academy of Sciences* **109**, 12974–
516 12979 (2012).
- 517 36. Glentis, A. *et al.* The emergence of spontaneous coordinated epithelial rotation on
518 cylindrical curved surfaces. *Science Advances* **8**, eabn5406.
- 519 37. Adams, C. L., Chen, Y.-T., Smith, S. J. & James Nelson, W. Mechanisms of Epithelial
520 Cell–Cell Adhesion and Cell Compaction Revealed by High-resolution Tracking of E-
521 Cadherin–Green Fluorescent Protein. *Journal of Cell Biology* **142**, 1105–1119 (1998).
- 522 38. Rhys, A. D. *et al.* Loss of E-cadherin provides tolerance to centrosome amplification in
523 epithelial cancer cells. *Journal of Cell Biology* **217**, 195–209 (2017).
- 524 39. Eisenhoffer, G. T. *et al.* Crowding induces live cell extrusion to maintain homeostatic cell
525 numbers in epithelia. *Nature* **484**, 546–549 (2012).
- 526 40. Marinari, E. *et al.* Live-cell delamination counterbalances epithelial growth to limit tissue
527 overcrowding. *Nature* **484**, 542–545 (2012).
- 528 41. Saw, T. B. *et al.* Topological defects in epithelia govern cell death and extrusion. *Nature*
529 **544**, 212–216 (2017).

- 530 42. Yang, Y.-A. *et al.* Local contractions regulate E-cadherin rigidity sensing. *Science Advances* **8**, eabk0387.
- 532 43. Nier, V. *et al.* Inference of Internal Stress in a Cell Monolayer. *Biophysical Journal* **110**,
533 1625–1635 (2016).
- 534 44. Sonam, S. *et al.* Mechanical stress driven by rigidity sensing governs epithelial stability.
535 *Nature Physics* **19**, 132–141 (2023).
- 536 45. Kong, W. *et al.* Experimental validation of force inference in epithelia from cell to tissue
537 scale. *Scientific Reports* **9**, 14647 (2019).
- 538 46. Paoli, P., Giannoni, E. & Chiarugi, P. Anoikis molecular pathways and its role in cancer
539 progression. *Biochimica et Biophysica Acta (BBA) - Molecular Cell Research* **1833**,
540 3481–3498 (2013).
- 541 47. Borghi, N. *et al.* E-cadherin is under constitutive actomyosin-generated tension that is
542 increased at cell–cell contacts upon externally applied stretch. *Proceedings of the
543 National Academy of Sciences* **109**, 12568–12573 (2012).
- 544 48. Schwartz, M. A. & DeSimone, D. W. Cell adhesion receptors in mechanotransduction.
545 *Current Opinion in Cell Biology* **20**, 551–556 (2008).
- 546 49. Liu, Z. *et al.* Mechanical tugging force regulates the size of cell–cell junctions.
547 *Proceedings of the National Academy of Sciences* **107**, 9944–9949 (2010).
- 548 50. Monfared, S., Ravichandran, G., Andrade, J. & Doostmohammadi, A. Mechanical basis
549 and topological routes to cell elimination. *eLife* **12**, e82435 (2023).
- 550 51. Durand, M. & Heu, J. Thermally Driven Order-Disorder Transition in Two-Dimensional
551 Soft Cellular Systems. *Phys. Rev. Lett.* **123**, 188001 (2019).
- 552 52. Park, J.-A. *et al.* Unjamming and cell shape in the asthmatic airway epithelium. *Nature
553 Materials* **14**, 1040–1048 (2015).

- 554 53. Cai, Y. *et al.* Nonmuscle Myosin IIA-Dependent Force Inhibits Cell Spreading and
555 Drives F-Actin Flow. *Biophysical Journal* **91**, 3907–3920 (2006).
- 556 55. Ellis, S. J. *et al.* Distinct modes of cell competition shape mammalian tissue
557 morphogenesis. *Nature* **569**, 497–502 (2019).
- 558 56. Onder, T. T. *et al.* Loss of E-Cadherin Promotes Metastasis via Multiple Downstream
559 Transcriptional Pathways. *Cancer Research* **68**, 3645–3654 (2008).
- 560 57. Ohsawa, S., Vaughen, J. & Igaki, T. Cell Extrusion: A Stress-Responsive Force for Good
561 or Evil in Epithelial Homeostasis. *Developmental Cell* **44**, 284–296 (2018).

562
563 **Acknowledgments:** We thank the members of the “Cell Adhesion and Mechanics” team for
564 helpful discussion. We acknowledge the ImagoSeine core facility of Institute Jacques Monod,
565 member of France-BioImaging (ANR-10-INBS-04) and IBiSA, with support of Labex “Who Am
566 I”, Inserm Plan Cancer, Region Ile-de-France and Fondation Bettencourt-Schueller. We thank
567 Tien Dang for establishing different cell lines. We thank Susana Godinho for sharing MCF10A
568 E-cad KO cells. We thank Wang Xi for providing soft hydrogels. We thank Matteo Spatuzzi for
569 help with data annotation. We thank Philippe Marcq for help with BISM.
570

571 **Funding:** This work was supported by the European Research Council (Grant No. Adv-
572 101019835 to B.L.), LABEX Who Am I? (ANR-11-LABX-0071 to B.L. and R.M.M.), the Ligue
573 Contre le Cancer (Equipe labellisée 2019), the CNRS through 80|Prime program (to B.L.),
574 Institut National du Cancer INCa (“Invadocad”, PLBIO18-236), and the Agence Nationale de la
575 Recherche (“MechanoAdipo” ANR-17-CE13-0012 to BL, “Myofuse” ANR-19-CE13-0016 to BL).
576 We acknowledge the ImagoSeine core facility of the IJM, member of IBiSA and France-
577 BioImaging (ANR-10-INBS-04) infrastructures. A.S. received funding from the CNRS 80|Prime
578 program and the Fondation Recherche Medicale (FDT-202404018282). L.A. received funding
579 from the Ligue contre le Cancer. A.D. acknowledges funding from the Novo Nordisk
580 Foundation (grant No. NNF18SA0035142 and NERD grant No. NNF21OC0068687), Villum
581 Fonden (Grant no. 29476), and the European Union (ERC, PhysCoMeT, 101041418). Views
582 and opinions expressed are however those of the authors only and do not necessarily reflect
583 those of the European Union or the European Research Council. Neither the European Union
584 nor the granting authority can be held responsible for them.
585

586 **Author contributions:** A.S., S.M., L.A., R.M.M., A.D. and B.L. designed the research. A.S. and
587 L.A. performed most and analyzed all the experimental data. S.M. performed phase field
588 simulations. C.R. performed tumor xenograft experiments. V.V. performed numerical
589 simulations. L.B. provided movies of WT/E-cad KO competition. E.M. provided patient tumor
590 samples. P.C. provided materials. A.S., S.M., L.A., R.M.M., A.D. and B.L. wrote the manuscript.
591 All authors read the manuscript and provided input on it.
592

593 **Competing Interests:** The authors declare no competing interests.

594

595 **Data and materials availability:** Data, materials and image analysis code are available upon
596 request.

597

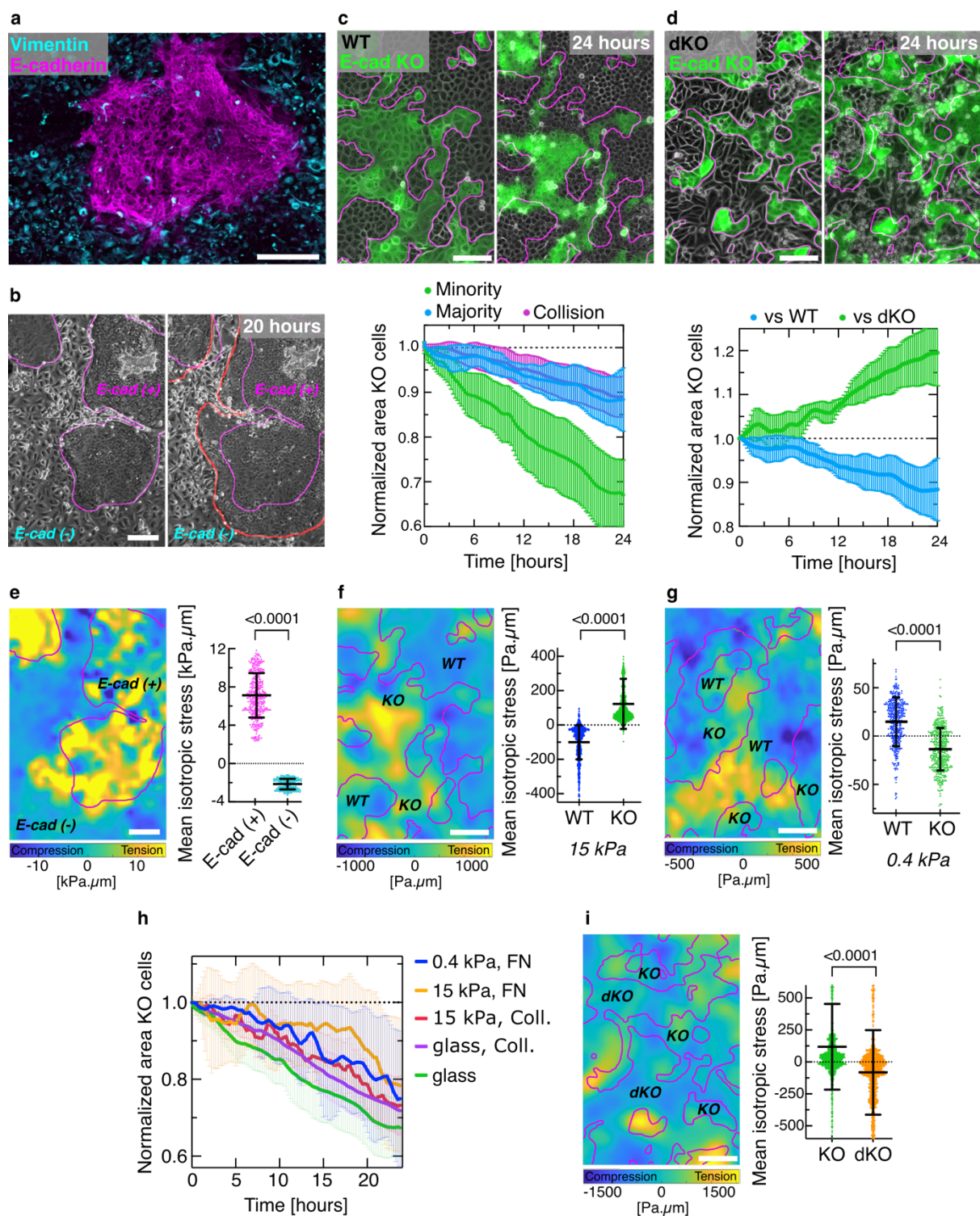
598 **Supplementary Materials:**

599

- 600 • Materials and Methods
601 • Figures S1 to S19
602 • Movies S1 to S9

603

604



605
606

607

Fig. 1: Intercellular force transmission capabilities provide a competitive advantage. **a**, Confocal image showing a monolayer of patient-derived metaplastic cancer cells. The E-cadherin positive (magenta) and vimentin positive (cyan) sub-populations sort completely. **b**, Phase contrast images of the cluster development within 20 hours. Red line shows cell clusters after 20 hours. **c**, Top: phase contrast and fluorescent images of a mixed culture of MDCK WT (grey) and MDCK E-cadherin knockout (green, fluorescently labelled with LifeAct-GFP) cells. Bottom: normalized area occupied by E-cad KO cells being in minority (green), majority (blue) or after the collision of two fully sorted populations (magenta). Collision assay realized through model wounds. Normalization to initial value, n=8 movies from N=3 independent experiments (Minority); n=6, N=3 (Majority); n=4, N=2 (Collision). **d**, Top: mixed culture E-cad KO cells (green) and E-cadherin / Cadherin-6 double knockout cells (dKO, grey). Bottom: normalized area of E-cad KO cells competing against WT (blue) or dKO (green) cells. Normalization to initial value, n=6 movies from N=3 independent experiments (vs WT); n=8, N=2 (vs dKO). **e**, Left: heatmap of the isotropic stress within metaplastic breast tumor tissue. The colormap shows compressive (blue) and tensile (yellow) stresses. The heatmap corresponds to the initial frame shown in **(b)**. Right: average isotropic stress for each cell type, n=5 movies from N=2 independent experiments. **f**, Left: heatmap of the isotropic stress within the competition between WT and E-cad KO cells on 15 kPa stiffness substrates. The heatmap corresponds to the initial frame shown in **(c)**. Right: average isotropic stress for each cell type, n=14 movies from N=4 independent experiments. **g**, Left: heatmap of the isotropic stress within the competition between WT and E-cad KO cells on soft substrates (370 Pa). Right: average isotropic stress for each cell type, n=7 movies from N=2 independent experiments. **h**, Normalized area occupied by E-cad KO cells on substrates with different stiffnesses and surface coatings (uncoated glass in green, glass coated with collagen in magenta, 15 kPa PDMS coated with fibronectin (FN) in orange, 15 kPa PDMS coated with collagen in red and 370 Pa PAA coated with FN in blue). E-cad KO cells are in minority. They are under tension on stiff and under compression on soft substrates. Normalization to initial value, n=8 movies from N=3 independent experiments (glass); n=7, N=1 (glass, Coll.); n=10, N=3 (15 kPa, Coll.); n=10, N=3 (15 kPa, FN) and n=10, N=3 (370 Pa). **i**, Left: heatmap of the isotropic stress within the competition between E-cad KO and dKO cells on 15 kPa stiffness substrates. The heatmap corresponds to the initial frame shown in **(d)**. Right: average isotropic stress for each cell type, n=13 movies from N=2 independent experiments. All datapoints represent the mean value of all isotropic stresses within one field-of-view of one frame. P-values from unpaired t-test. All magenta lines show initial cell clusters. All error bars show the standard deviation. Scale bars 200 μ m (**a, b, e**); 100 μ m (**c, d, f, g, i**).

608

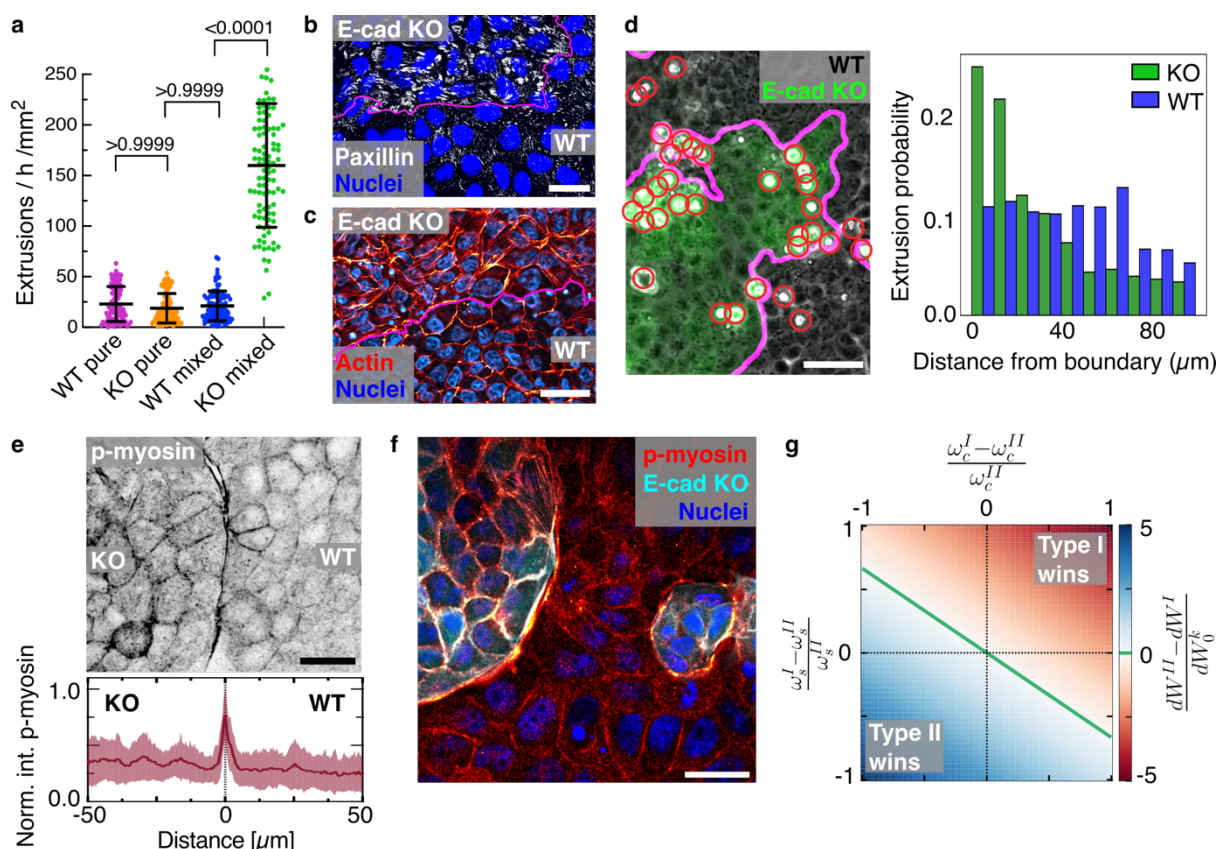
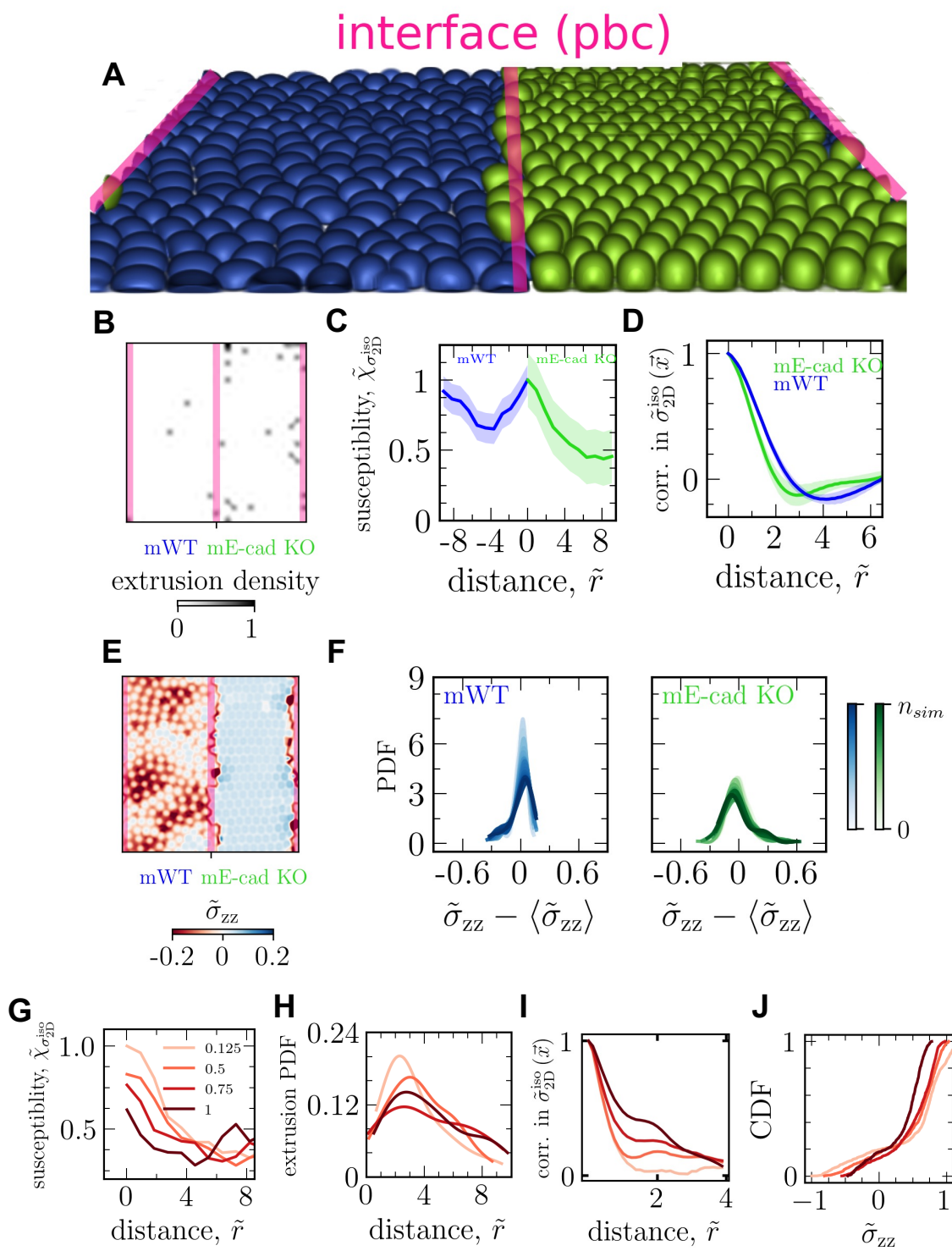
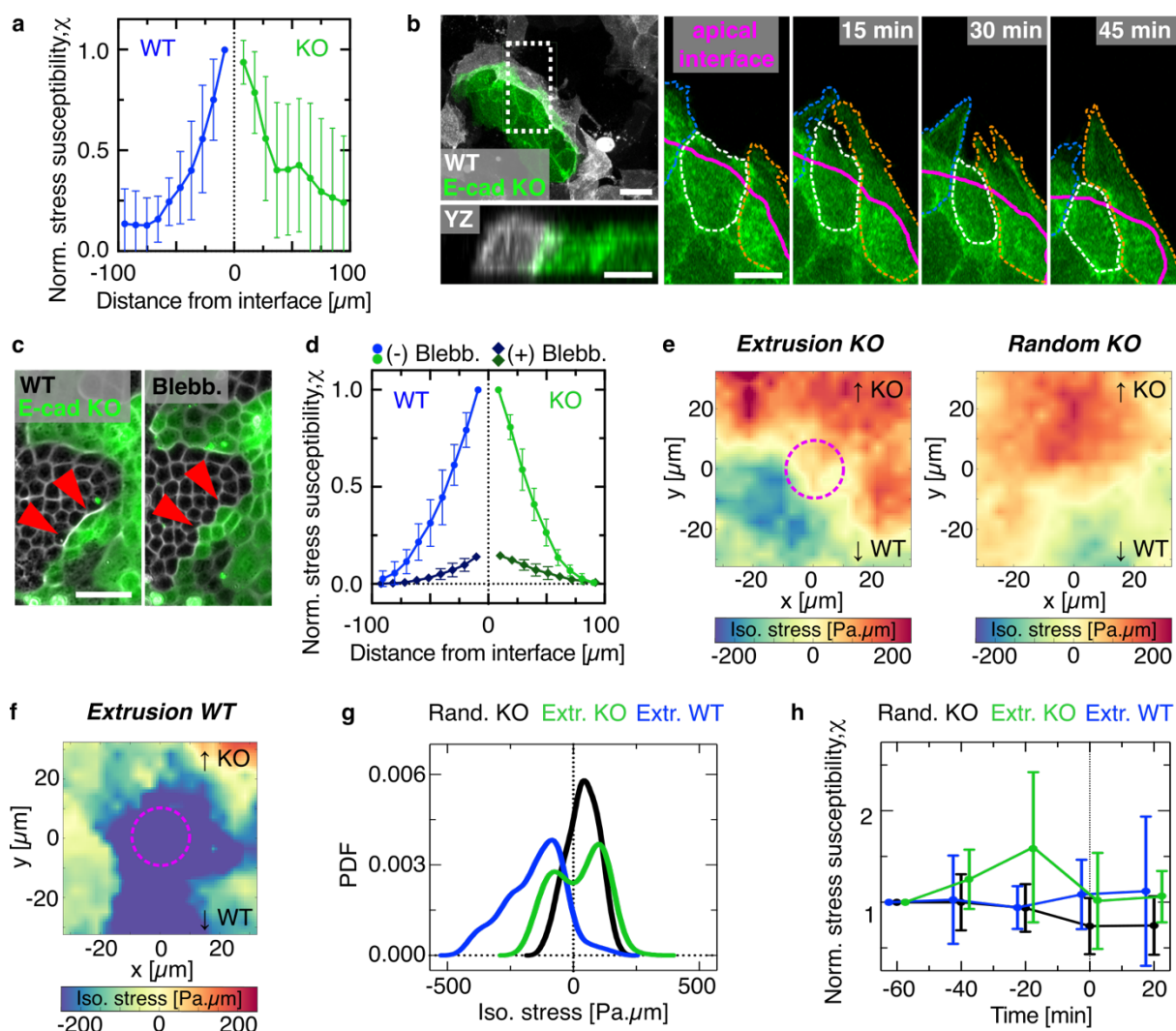


Fig. 2: E-cad KO cells are eliminated at a mechanically active interface. **a**, Extrusion rates calculated by counting all extrusions within 1-hour intervals normalized to the area occupied by each cell type during the time interval. E-cad KO cells are in minority in the mixed culture. P-values from Kruskal-Wallis test corrected for multiple comparisons (Dunn's test). Extrusions quantified for n=100 intervals representing 8 movies from N=2 (pure cultures) or N=3 (mixed cultures) independent experiments. **b**, Relative mechanical properties of E-cad KO cells. Example images of Focal Adhesions (Paxillin, white) and **c**, the actin cytoskeleton (red, maximum projection). **d**, Left: representative phase contrast and fluorescent image of MDCK WT and E-cad KO cells (green). Red circles indicate extrusions. Right: probability distribution of cell extrusion regarding the distance from the interface for WT and E-cad KO cells. Cells have a typical diameter of 10-15 μm . n=14729 KO extrusion, n=11031 WT extrusion, from N=4 independent experiments. **e**, Top: inverted grayscale image of phospho-myosin at the tissue interface. Bottom: normalized intensity of phospho-myosin obtained from line plots crossing the tissue interface. Lines were centered at the interface (dashed line, distance=0), indicated by fluorescent signal from E-cad KO lifeAct-GFP (not shown), averaged from n=24 measurements from N=2 independent experiments. **f**, Example fluorescent image of pluricellular actomyosin cables forming in WT cells observed in coculture. Cables are enriched in phospho-myosin (red, intensity-coded) and form along islands of E-cad KO cells (cyan). **g**, Phase diagram showing the work required to eliminate cells. X-axis shows the difference in cell-cell adhesion. Y-axis shows the difference in cell-substrate adhesion. Color code indicates difference in work, i.e. indicates winning and losing. The top left region shows that cells with relative high cell-cell adhesion can win despite lower relative cell-substrate adhesion. All error bars show the standard deviation. Scale bars 50 μm (**d**); 25 μm (**c**, **f**); 10 μm (**b**).



610
611

Fig. 3: Computational model reveals the role of high fluctuations at the active interface in determining the outcome of cell competition. **a**, Example simulation snapshot with mE-cad KO cells (Green) losing to mWT cells (Blue) at the interface (red lines), keeping in mind the periodic boundary conditions (PBC). **b**, Extrusion density map representing spatial distribution of extrusion events, corresponding to the simulation in **(a)**. **c**, Susceptibility of two-dimensional, i.e. in-plane, isotropic stress field and the out-of-plane component of stress tensor normalized by the maximum value in mE-cad KO cells for each, as a function of distance from the interface. The distance is normalized by the initial cell radius. The data corresponds to the simulation in **(a)**. **d**, Spatial correlation of the in-plane, i.e. two-dimensional, isotropic stress for each cell type corresponding to the simulation in **(a)**. **e**, Out-of-plane stress component field, normalized by maximum value of in-plane compression. **f**, Probability density function (PDF) for fluctuations in out-of-plane stress component, normalized by maximum value of in-plane compression for each cell type near the interface within the distance of four times cell radius on each side. The color shades capture the temporal evolution of the PDFs where is the total number of time steps. **g**, Susceptibility of in-plane isotropic stress field for mE-cad KO cells for fixed cell-substrate adhesion and various cell-cell adhesion strengths ($\tilde{\omega}_{cc}$) normalized by the value for the lowest cell-cell adhesion at the interface. **h**, Extrusion PDFs corresponding to **(g)**. **i**, Spatial correlations corresponding to coarse-grained in-plane isotropic stress fields averaged, ensemble and temporal, centered around an extruding cell in a square domain of eight times cell radius for fixed cell-substrate adhesion and varying cell-cell adhesions corresponding to **(g)**. **j**, cumulative distribution functions (CDF) corresponding to the average out-of-plane stress fields normalized by maximum in-plane compression around an extruding cell, showing higher localization for lower cell-cell adhesion: the peak shifts to the left and becomes less tensile as cell-cell adhesion increases.



612

Fig. 4: E-cad KO cells are eliminated through increased stress fluctuations. **a**, Isotropic stress susceptibility as a function of the distance from the interface for each cell type normalized to the maximum value. n=18 movies from N=5 independent experiments including mixed cultures and collisions. **b**, Snapshots of actin dynamics at the interface. Maximal projections and side view of MDCK E-cad KO LifeAct-GFP (green) and MDCK WT LifeAct-Ruby (white). Right: Zoom-in on maximal projection of E-cad KO cells protruding below WT cells. Apical interface indicated by magenta line drawn based on WT LifeAct-Ruby signal (not shown). **c**, Phase contrast and fluorescent image of the boundary (red arrows) before (left) and 2 hours after 20 μm blebbistatin addition (right). **d**, Isotropic stress susceptibility versus distance from the interface for each cell type, before (dots) and after (rectangles) addition of blebbistatin and normalized to the highest value. n=10 movies from N=2 independent experiments. **e**, Left: ensemble average heatmap of the local isotropic stress before E-cad KO extrusions. Extrusions considered were within a 30 μm distance from the interface and stresses were averaged up to 40 min before automated detection of the extrusion, excluding the timepoint of completed extrusion. Stress fields were oriented based on E-cad KO fluorescent signal so that the KO side is on top and the WT side on the bottom (see Methods). Right: average heatmap of the isotropic stress within a square of size 30 μm around random position in E-cad KO occupied area within a 30 μm distance from the interface. n=798 extrusions (E-cad KO), n=750 KO random positions from 4 independent experiments. **f**, Average heatmap of the isotropic stress before WT bulk extrusions. n=741 extrusions from N=4 independent experiments. **g**, Probability density functions of the average isotropic stress distribution before extrusion detection (WT cells bulk elimination, blue, KO cells interface elimination, green, and random KO interface position, black) corresponding to **(e, f)**. **h**, Temporal evolution of the mean isotropic stress susceptibility before ($t < 0$) and briefly after an extrusion event. t=0 indicates timepoint of automated detection of extrusion. Random position of E-cad KO cells at the interface: black, E-cad KO elimination: green, WT cell elimination: blue. Susceptibility is averaged within a square of size 60 μm around one extrusion event. Normalized to initial value, n=726 extrusions (E-cad KO), n=1050 KO random positions and n=334 extrusions (WT) in n=6 movies from N=2 independent experiments. All error bars show the standard deviation. Scale bars 50 μm (**c**); 10 μm (**b**).

613

614

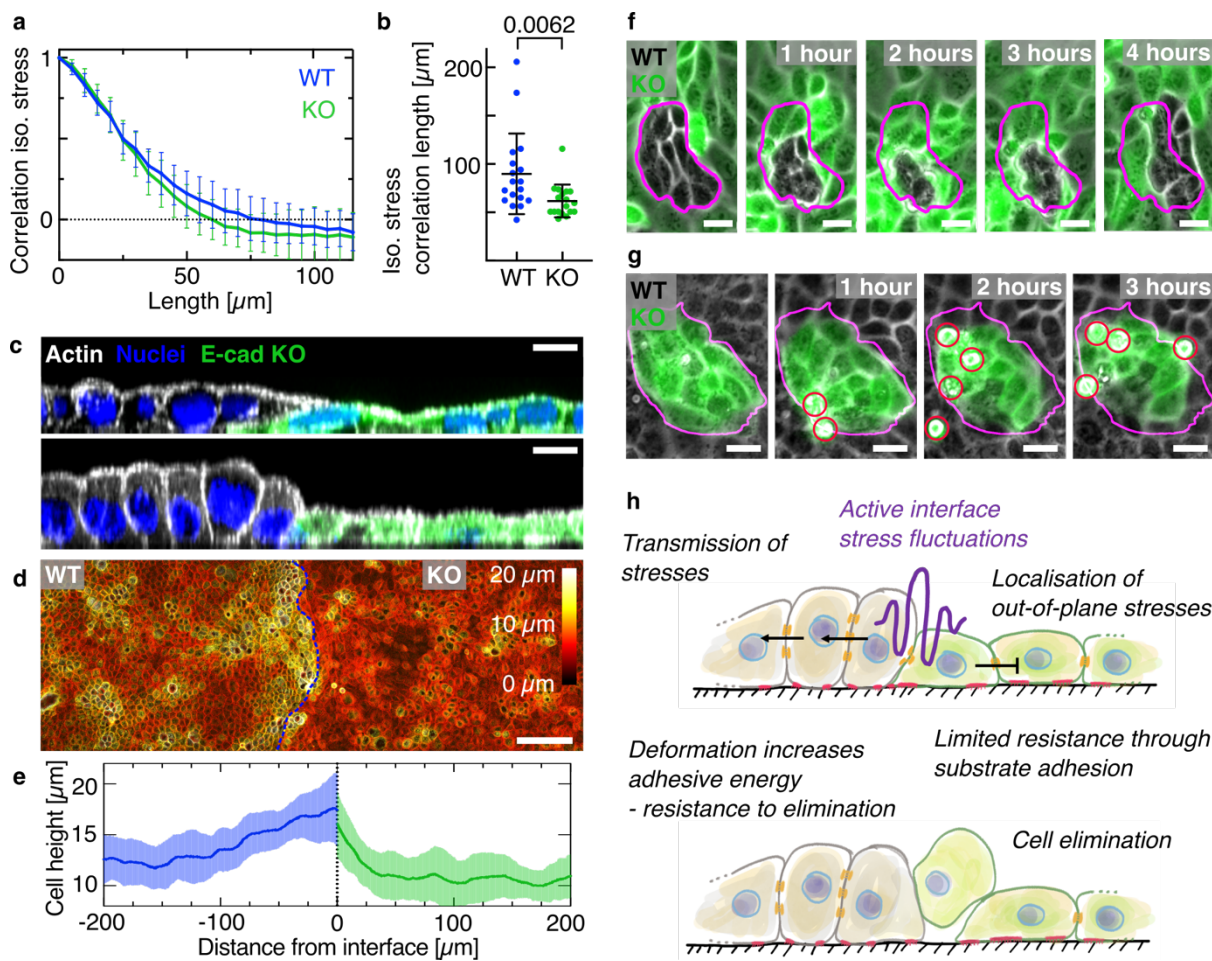


Fig. 5: Increased intercellular adhesion endows cells with increased resistance to elimination. **a**, Spatial auto-correlation of the isotropic stress for each cell type. The zero-crossing indicates the correlation length. $n=18$ movies from $N=5$ independent experiments. **b**, Average correlation length of the isotropic stress for each cell type. P-value from unpaired t-test. **c**, Deformation of WT cells close to the interface. Confocal image showing side views of actin (white), lifeAct-GFP in E-cad KO cells (green) and the nuclei. Top: Example cell height in mixed culture. Bottom: Infrequent increased height for WT cells. **d**, Color-coded height projection of actin signal in collision assay. **e**, Quantification of cell height in collision. E-cad KO cells exhibits a faster decrease of cell height with distance from the interface compared to WT. $n=15$ positions from $N=2$ independent experiments. **f**, Brightfield and fluorescent (E-cad KO, green) images of WT cells getting compacted without cell elimination. **g**, E-cad KO cells responding to island compaction through cell elimination. **h**, Sketch of proposed mechanism. All error bars show the standard deviation. Scale bars 100 μm (**d**); 20 μm (**g**); 10 μm (**c**, **f**).